

Journal of Biomedical Optics

BiomedicalOptics.SPIEDigitalLibrary.org

Influence of material and haptic design on the mechanical stability of intraocular lenses by means of finite-element modeling

Laura Remón
Damian Siedlecki
Iulen Cabeza-Gil
Begoña Calvo

SPIE.

Laura Remón, Damian Siedlecki, Iulen Cabeza-Gil, Begoña Calvo, "Influence of material and haptic design on the mechanical stability of intraocular lenses by means of finite-element modeling," *J. Biomed. Opt.* **23**(3), 035003 (2018), doi: 10.1117/1.JBO.23.3.035003.

Influence of material and haptic design on the mechanical stability of intraocular lenses by means of finite-element modeling

Laura Remón,^{a,*} Damian Siedlecki,^b Iulen Cabeza-Gil,^c and Begoña Calvo^{c,d}

^aUniversidad de Zaragoza, Departamento de Física Aplicada, Facultad de Ciencias, Zaragoza, España

^bWroclaw University of Science and Technology, Visual Optics Group, Department of Optics and Photonics, Wroclaw, Poland

^cUniversidad de Zaragoza, Escuela de Ingeniería y Arquitectura (EINA), Aragón Institute of Engineering Research (I3A) Maria de Luna s/n, Campus Río Ebro, Edificio "Agustín de Betancourt", Zaragoza, España

^dCentro de Investigación Biomédica en Red en Bioingeniería, Biomateriales y Nanomedicina (CIBER-BBN), Spain

Abstract. Intraocular lenses (IOLs) are used in the cataract treatment for surgical replacement of the opacified crystalline lens. Before being implanted they have to pass the strict quality control to guarantee a good biomechanical stability inside the capsular bag, avoiding the rotation, and to provide a good optical quality. The goal of this study was to investigate the influence of the material and haptic design on the behavior of the IOLs under dynamic compression condition. For this purpose, the strain–stress characteristics of the hydrophobic and hydrophilic materials were estimated experimentally. Next, these data were used as the input for a finite-element model (FEM) to analyze the stability of different IOL haptic designs, according to the procedure described by the ISO standards. Finally, the simulations of the effect of IOL tilt and decentration on the optical performance were performed in an eye model using a ray-tracing software. The results suggest the major importance of the haptic design rather than the material on the postoperative behavior of an IOL. FEM appears to be a powerful tool for numerical studies of the biomechanical properties of IOLs and it allows one to help in the design phase to the manufacturers. © 2018 Society of Photo-Optical Instrumentation Engineers (SPIE) [DOI: [10.1117/1.JBO.23.3.035003](https://doi.org/10.1117/1.JBO.23.3.035003)]

Keywords: finite-element modeling; biomechanical stability; haptic design; mechanical properties; optical performance.

Paper 170657R received Oct. 9, 2017; accepted for publication Feb. 12, 2018; published online Mar. 5, 2018.

1 Introduction

Nowadays, it is possible to achieve complete spectacle independence after cataract surgery due to improvements in several aspects, which include surgical techniques (control of the corneal aberrations), accuracy of preoperative measurements (biometry), intraocular lens (IOL) design, and technology development. The evolution of IOL optical designs, such as multifocal intraocular lenses (MIOLs)¹ and toric intraocular lenses (T-IOLs),² provides the patients good vision, not only for far, such as the monofocal IOLs, but also for near and intermediate objects and the possibility to correct the preexisting corneal astigmatism.

Nevertheless, many other factors need to be taken into account when selecting a particular IOL to be implanted in the treatment of cataracts. Material properties and haptic designs are of key importance for evaluation of the biomechanical stability of the intraocular implants inside pseudophakic eyes.^{3,4} On one hand, materials should be as inert and stable as possible and biocompatible to prevent the posterior capsule opacification (PCO). On the other hand, they have to be easy to handle concerning folding and implantation. Several studies have demonstrated that hydrophobic materials are associated with lower PCO than the hydrophilic.^{5,6} A sharp square edge design is thought to reduce risk of PCO compared with round optic edge.^{7,8}

Another important issue about the IOL material is its capacity to recover its optical properties after implantation. It has been reported that the time of folding and unfolding of the hydrophobic material is significantly longer than for the hydrophilic material or silicone material, being smaller for silicone lenses, which is claim to be more elastic and seems to have a better shape memory.^{9,10} IOLs fabricated with hydrophobic materials require a higher force and longer relaxation time injected to restore their desired shape.^{9,10} Bozukova et al.⁹ explained in detail the parameters on which this behavior depends for both types of materials.

The main function of haptics is to provide the proper positional stability to avoid the tilt and decentration of IOL, which may affect the optical performance, particularly in multifocal¹¹ and toric designs of IOLs. The optical performance metrics must satisfy the minimum requirements set out by the International Standards ISO 11979-2:2014.¹² Rotation around the optical axis is a major issue for toric IOL and the rotational stability may be crucial for good visual outcome. Patel et al.¹³ compared silicone loop haptics with silicone plate haptics and reported better rotational stability of the silicone plate haptics. Another study¹⁴ found that acrylic plate- and loop-haptics have similar rotational stability. Chang¹⁵ found that the silicone plate haptics have a higher incidence of rotation than hydrophobic C-loop. Zhong et al.¹⁶ found that single-piece IOLs exhibit better axial stability and more stable refractive outcome than three-piece IOLs. Rotation occurs most frequently in the early postoperative

*Address all correspondence to: Laura Remón, E-mail: lauremar@unizar.es

period, before anterior and posterior capsules fuse together with the lens.¹⁷ The strength of IOL adhesion to the bag varies: hydrophobic implants have the highest adhesive properties, followed by the hydrophilic ones, then the polymethyl methacrylate (PMMA) IOLs, and finally the silicone IOLs.^{18,19} In addition, the lens design and the size of the capsule bag can play an important role in rotation of the implants inside the pseudophakic eye. IOLs with smaller diameters²⁰ and larger capsule bags of the patient's eye may be the factors to increase the risk of IOL rotation.

There are several methods to measure IOL decentration and tilt once it is implanted inside the pseudophakic eyes. These include slit lamp assessment,²¹ retroillumination photography,²² Scheimpflug imaging,¹⁶ optical coherence tomography,^{23–25} and measurements using Purkinje reflections.^{26–28} But before the implant injection into the eye, a study on reliable prediction of the visual outcome of the implantation needs to be performed. Up to now, many efforts have been made to predict the postoperative visual quality of the pseudophakic eyes. Most studies focus either on the optimization of the optical geometry of the IOL^{29–32} or the influence of the postoperative lens position on the optical performance.^{28,33,34}

To reliably predict the postoperative optical performance and the mechanical behavior of the intraocular implant, it is required for IOL to have strict quality and performance features, which may be useful for this prediction. This stage is of major importance if the implantation is aimed to be a safer and even more effective method of cataract treatment. IOL designs must fulfill the strict requirements in terms of the optical performance (resolution efficiency or modulation transfer function), and in terms of mechanical properties, e.g., compression force, dimension tolerance, and dynamic fatigue durability. The ISO 11979-

3:2012³⁵ specifies requirements of the test methods for certain mechanical properties of IOLs. There are several studies,^{4,9,10} which have experimentally evaluated the biomechanical properties of different IOLs.

The purpose of the present study is to evaluate the biomechanical stability of four different IOLs of hydrophobic and hydrophilic materials with different optic and haptic designs using the finite-element model (FEM). The mechanical behavior of the materials was experimentally evaluated by an uniaxial compression relaxation test in a saline bath. The tests were performed according to the procedure described by ISO11979-3,³⁵ which establishes the compression of the IOL haptics until 10 mm for IOLs intended for capsular bag placement. The different parameters described in the ISO standard were evaluated along with the test. To our best knowledge, it is the first time that the behavior of different IOLs designs under dynamic compression conditions has been modeled using FEM. Also, the optical properties were evaluated with the use of pseudophakic eye model by means of ray-tracing software for the initial and final positions of the IOLs, resulting from the FEM modeling. The obtained results were discussed with *in vitro* and *in vivo* data presented in other studies.

2 Methods

2.1 Mechanical Characterization of Materials

Two different materials provided by Benz Research and Development have been evaluated: (a) hydrophobic acrylic material (Benz HF-1.2 Natural Yellow™) with a water uptake of <4% and a refractive index of 1.485 at 35°C ($\lambda = 546$ nm); this material contains ultraviolet-A (UV-A)





Feature	Model A	Model B	Model C	Model D
Product				
Material	Hydrophobic Hydrophilic	Hydrophobic	Hydrophobic	Hydrophobic
Overall design	Single piece	Single piece	Single piece	Single piece
Design concept	Aberration free	Aberration free	Aberration free	Aberration free
Haptic type	C-loop	C-loop	Plate	Plate with a hole
Haptic angulation [deg]	0	5	0	0
Optic size [mm]	6.00	6.00	6.00	6.00
Overall size [mm]	13.00	12.50	10.75	10.75

Fig. 1 Properties of the IOLs under consideration.

blocking and violet filtering monomer (Natural Yellow™ patented by Benz, U.S. Patent 7,947,796) and (b) hydrophilic acrylic material (Benz IOL 25 CLUV) with a water uptake of $25.5\% \pm 2$ and a refractive index of 1.462 at 35°C ($\lambda = 546 \text{ nm}$); this material blocks UV-A light only (clear UV).

To evaluate the mechanical response of hydrophobic and hydrophilic materials, five disks of 3.00-mm thickness and 15.00 mm of diameter were tested with Instron 5548 Microtester with a 50 N full-scale load cell. Before the experiments, the sample disks were submerged in a saline solution for 72 h. The material in this device is tested in uniaxial compression relaxation test in a saline bath. Three preconditioning cycles performed at 5.00 mm/min displacement rate, until 20% deformation, that preceded the 2.5 h relaxation phase were applied. Using the Instron software, the force–displacement responses were acquired. From the recorded data, strain is calculated as: $\lambda = \Delta L/L_0$, where ΔL is the measured displacement and L_0 is the initial thickness in dry conditions. Engineering stress is calculated as: $P = N/A_0$, where N is the load registered and A_0 is the initial cross-sectional area of the sample normal to the loading direction.

2.2 Intraocular Lenses

Four monofocal aspheric IOLs to be implanted in capsular bag with different haptic designs and different overall diameters were analyzed. Figure 1 shows the main properties of the IOLs evaluated in this study: (1) model A is a single-piece IOL with non-angulated C-loop haptics; it has an overall diameter of 13.00 and 6.00 mm of optical diameter; (2) model B is a single-piece IOL with modified 5-deg angulated C-loop haptics; it has an overall diameter of 12.50 and 6.00 mm of optical diameter; (3) model C is a single-piece IOL with plate haptics within perforation; and (4) model D is a single-piece with plate haptics with a small hole (area hole is 3.24 mm²). Model C and model D have an overall diameter of 10.75 and 6.00 mm of optical diameter. The model A was analyzed with both hydrophobic and hydrophilic materials, and the other models only with hydrophobic material.

All the lenses have an aberration-free aspheric IOL designs with a prolate anterior lens surface and no inherent spherical aberration. The power of the tested IOLs was +22.00 diopters (D).

2.3 In Silico Evaluation of Compression Test

Numerical simulation of the biomechanical behavior of the IOLs during a compression test was performed by the finite-element method (FEM) using Abaqus 6.14 software. The tests were performed according to the procedure described by ISO11979-3,³⁵ which establishes the compression of the IOL haptics until 10 mm for IOLs intended for capsular bag placement. The IOL was placed between two clamps with faces having a radius of 5.00 mm and a distance approximately equal to the overall dimension of the IOL called reference configuration [see Fig. 2(a)]. The clamps were considered as rigid solids and the IOLs as a deformable material. The left clamp was fixed, and the right ones were moved until the 10-mm haptic compression with a rate of 0.1 mm/s by an implicit dynamic analysis [see Fig. 2(b), which presents the final configuration].

In this configuration, the following parameters were measured: the compression force measured at the horizontal plane, the axial shift measured at the vertical plane [see

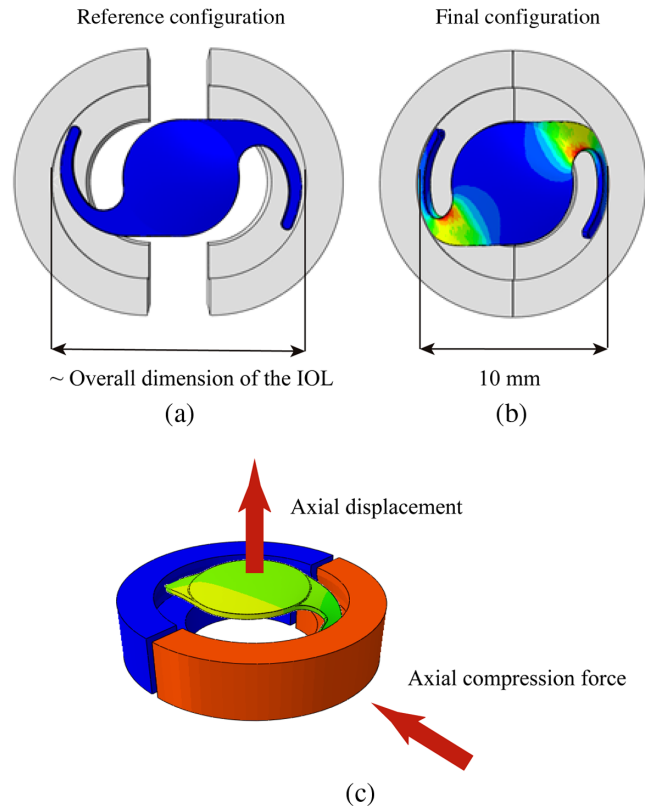


Fig. 2 (a) Reference (initial) configuration: distance between clamps, approximately equal to the overall dimension of the IOL. (b) Final configuration: distance between clamps equals to 10 mm following the procedure described in the ISO 11979-3. (c) Representation of the IOL and clamps used for the finite elements numerical simulation, axial compression force, and axial displacement are shown.

Fig. 2(c)], the lateral decentration in x - and y -directions, the tilt in both x - and y -directions, and the angle of contact between the lens and the clamp. These parameters were evaluated in the reference configuration, in the final one as well as in the intermediate positions all along the test.

Quadratic full integration mixed formulation solid elements (C3D10H) were used to perform the simulations. A sensibility analysis of the mesh, with different mesh densities, was performed to minimize the computational cost (simulation time) and to get a reliable result. The final mesh density for each IOL is shown in Fig. 3.

Certain areas, such as the haptic zones, required a higher mesh resolution because of the contact between the haptics and the clamps.

2.4 Optical Modeling

To estimate the effect of displacement of IOLs on the optical performance, a numerical model of a pseudophakic eye was implemented to optical analysis software (Zemax LLC) and the ray-tracing simulations were performed. The model was based on the emmetropic Atchison schematic eye (see Table 1 for details),³⁶ where the gradient index crystalline lens was replaced with a particular IOL to estimate the image quality deterioration being the result of the IOL displacement. Following the procedures presented in earlier studies,²⁸ for the purposes of optical performance simulations, the initial position

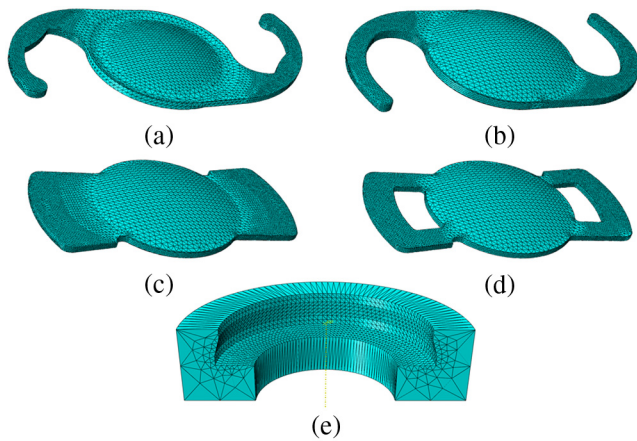


Fig. 3 FEM of the IOLs under consideration and one of the clamps. (a) Model A: 61,585 nodes and 66,708 elements; (b) model B: 26,109 nodes and 32,908 elements; (c) model C: 36,616 nodes and 35,900 elements; (d) model D: 47,237 nodes and 35,297 elements; and (e) clamp: 1831 nodes and 8281 elements.

Table 1 Parameters of the emmetropic eye model followed from the refractive error-dependent model described by Atchison.³⁶

Medium	Radius [mm]	Conic constant	Thickness [mm]	Refractive index at 555 nm
Anterior cornea	7.77	-0.15	0.55	1.376
Posterior cornea	6.40	-0.275	3.15	1.3374
Pupil	Infinity	0	0	1.3374
Anterior lens	11.48	-5.00	1.44	Grad A ^a
Equator	Infinity	0	2.16	Grad P ^b
Posterior lens	-5.90	-2.00	16.28	1.336
Retina	$R_x = -12.72$ $R_y = -12.91$	$k_x = 0.25$ $k_y = 0.27$	—	—

$${}^a\text{Grad A} = 1.371 + 0.0652778z - 0.0226659z^2 - 0.0020399(x^2 + y^2)$$

$${}^b\text{Grad P} = 1.418 - 0.0100737z^2 - 0.0020399(x^2 + y^2)$$

of the IOL within the pseudophakic eye model was optimized so that its anterior principal plane coincided with the anterior principal plane of the crystalline lens of the original, phakic model.

The magnitude of the IOL displacement (at the point of final configuration, where the distance between the clamps is equal to zero), namely tilt around the x - and y -axes, decentration along the x - and y -axes were adapted according to the characteristics resulted directly from the FEM modeling, presented in Sec. 4. The axial displacement was not taken into account in the optical performance simulations intentionally since it only produces a defocus (about 1.5 D for 2 mm of axial displacement), which masks the effects induced by decentration and tilt of the IOL. In a real pseudophakic eye, this defocus is associated with the refractive error, which is usually corrected by means of spectacle correction.

The optical performance of the pseudophakic eye model was estimated in terms of several quantities, namely (a) the area under modulation transfer function (MTF_a) for the range frequencies of 0 to 30 and 0 to 60 cycles per degree and (b) Zernike wavefront aberration coefficients associated with defocus (Z_2^0), astigmatism (Z_2^{-2} and Z_2^2), primary coma (Z_3^{-1} and Z_3^1), and spherical aberration (Z_4^0). For the purposes of all the optical performance simulations, the diameter of the physical pupil was set to 3 mm and the wavelength was 555 nm.

The optical performance estimation was performed for all the IOLs under consideration.

3 Results

3.1 Mechanical Properties of Materials

Although both the hydrophobic and hydrophilic materials present a viscoelastic behavior, in this work only the elastic response has been modeled. The average elastic responses for both materials are presented in Fig. 4 by the uniaxial stress–strain curves in compression and assuming the same behavior in tension. The material response exhibited a nonlinear behavior, modeled by an isotropic–incompressible hyperelastic model. The experimental results can be successfully approximated by a polynomial, $N = 2$, strain-energy function (see Fig. 4)

$$W = C_{10}(I_1 - 3) + C_{01}(I_2 - 3) + C_{11}(I_1 - 3) + C_{20}(I_1 - 3)^2 + C_{02}(I_2 - 3)^2,$$

where I_1 , I_2 are the strain invariants of the symmetric right Cauchy–Green tensor, and C_{ij} are the material constants. The values of the C_{ij} parameters for the materials under consideration are given in Table 2.

As shown in Fig. 4, the hydrophobic material is more rigid than the hydrophilic.

3.2 In Silico Evaluation of Compression Test

Our first goal of this part of the study was to evaluate the behavior of the same design of IOL (model A) made of both materials: hydrophobic and hydrophilic. Figure 5 shows the evolution of

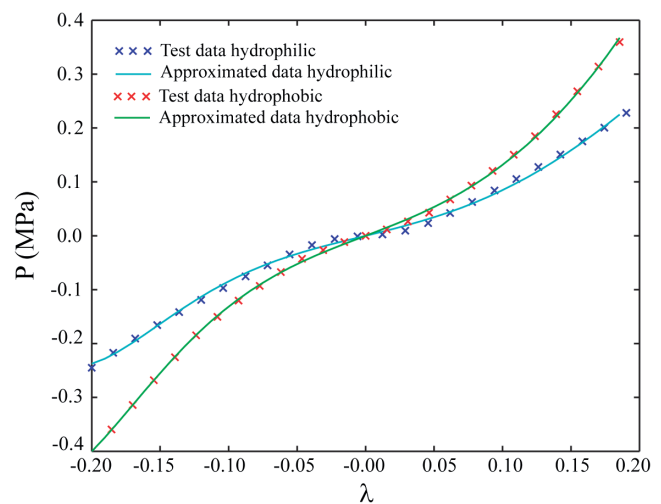


Fig. 4 Stress–strain characteristics for the two different materials under consideration. Test data and their approximations data are shown.

Table 2 Materials constants for both materials under consideration. The units are MPa.

Material	C_{01}	C_{10}	C_{11}	C_{20}	C_{02}
Hydrophobic	0.36	-0.19	13.14	-5.02	-7.09
Hydrophilic	0.25	-0.14	-7.54	16.75	-8.50

the compression force (left y-axis) and the axial displacement (right y-axis) as a function of the clamp displacement. As it can be observed in the figure, the compression force simulated numerically for the hydrophilic IOL was slightly lower than for the IOL made of hydrophobic material. This is a direct consequence of the measured materials properties (see Table 1). The compression force when the haptic is maximally compressed is 2.039 and 3.172 mN for the hydrophilic and the hydrophobic material, respectively. The axial displacement was the same for both materials 1.91 mm.

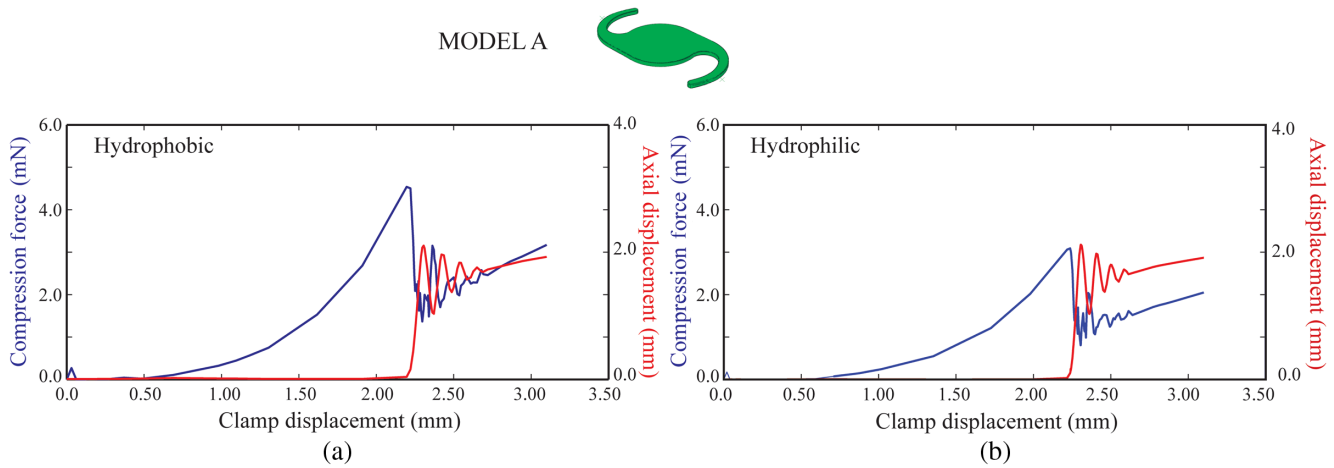


Fig. 5 (a) Evolution of the compression force (blue line, y-axis) and (b) the axial displacement (red line, y-axis) as a function of the clamp displacement for the model A IOL made of different materials: (a) hydrophobic material and (b) hydrophilic material. The compression force was measured until the haptics compressed to a diameter of 10 mm following the procedure described in the ISO 11979-3.

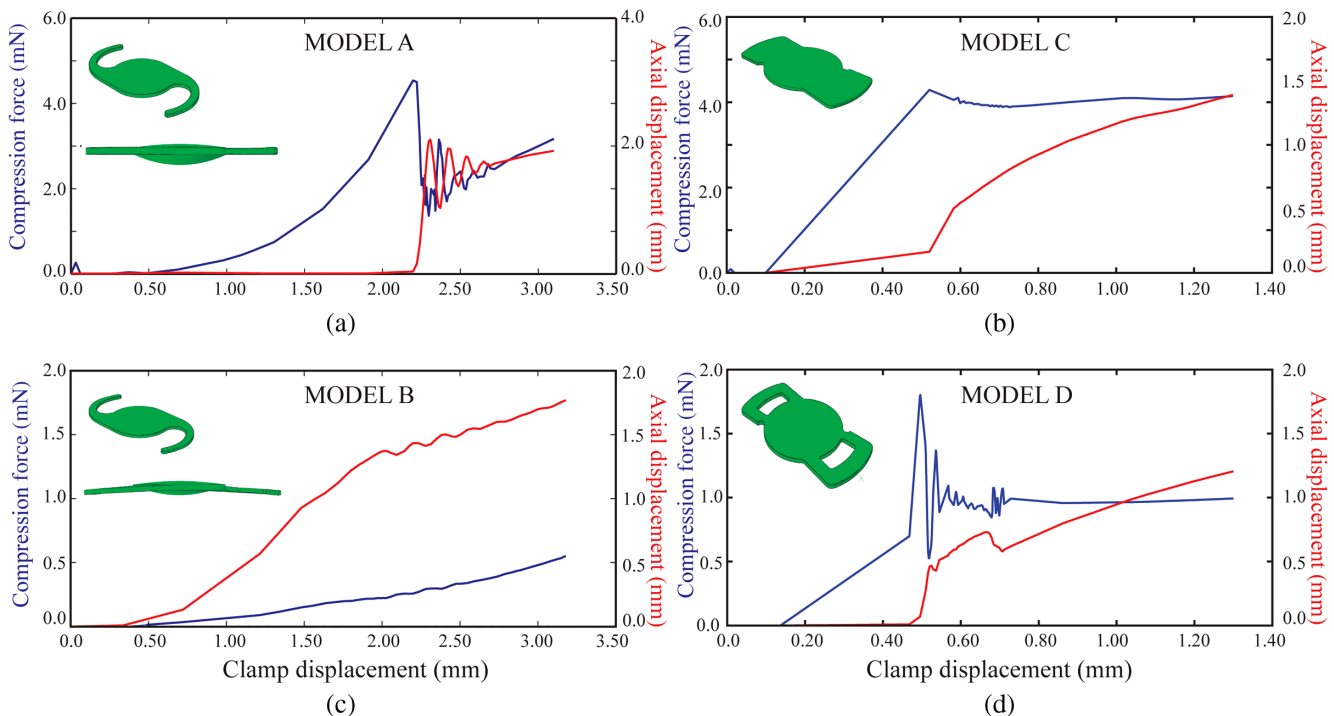


Fig. 6 (a) Evolution of the compression force (y-axis) and (b) axial displacement (y-axis) as a function of the clamp displacement for different models of IOLs made of the same hydrophobic material. The compression force was measured until the haptics compressed to a diameter of 10 mm following the procedure described in the ISO 11979-3.

The second goal of this part of the study was to compare the biomechanical properties for each IOL design, having different haptic designs, under the condition that all of them are made of the same material (hydrophobic). Figure 6 shows the evolution of the compression force (left y-axis) and the axial displacement (right y-axis) as a function of the clamp displacement for each of the IOL models under consideration. For the plate-haptic IOLs, the magnitude of the total clamp displacement is lower because of their smaller overall diameter (see Fig. 1). The presented characteristics clearly show that compression force and axial displacement depend significantly on the haptic design of the IOL. The axial displacement and the compression force have almost a linear behavior for the models B and C, whereas the other models reveal a larger instability during the process. The largest compression force is manifested for the models A and C. Table 3 shows the compression force and the axial displacement at the final configuration for each model of the IOL. The range of compression force variation was from 0.518 mN for the model B to 4.143 mN for model C. The numerically estimated axial displacement was very similar for all model IOLs, being slightly larger for the C-loop IOLs.

The decentration and tilt of the IOLs were calculated according to the procedure recommended by the ISO 11979-3.³⁵

Figure 7 shows the obtained results as a function of the clamp displacement. The optic decentration was estimated as the distance between the optic center of the IOL and the geometrical center of the two clamps. Such large peaks at the beginning of the decentration characteristics are the result of the distance between the round edges between the clamps being larger than the overall diameters of the IOLs. The characteristics obtained for the model A and both materials are very similar. Table 3 shows optic decentration and optic tilt values at the actual reference. All these values are largely lower than the tolerance limits acceptable by the current ISO standard. The highest value of the optic decentration and optic tilt at intermediate positions is obtained by the model A. The angle of contact is also shown in this table for each model. The range of angle contact variations was between 131 deg and 86 deg.

3.3 Optical Performance Simulations

Table 4 shows the relative values of the area under MTF calculated as the fraction of the area under MTF for the final configuration (with the displacement parameters seen in Table 3, only the axial displacement was set to 0) compared with the area under MTF for the initial (reference) configuration (which

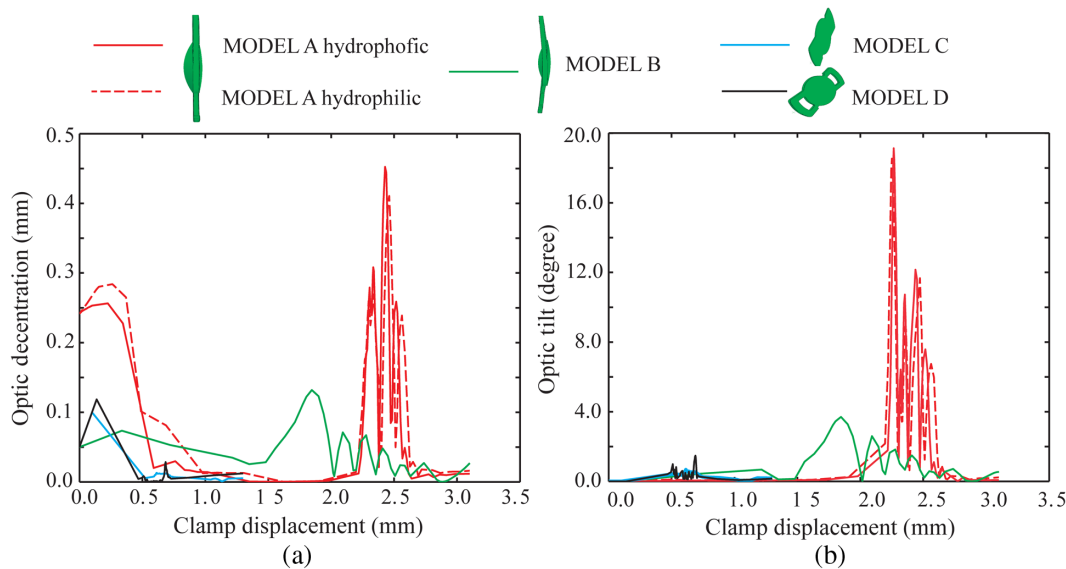


Fig. 7 Evolution of (a) the optic decentration and (b) the optic tilt as a function of the clamp displacement for different models of IOLs.

Table 3 Force and displacement parameters estimated for each IOL at the final configuration.

Material	Compression force [mN]	Axial displacement [mm]	Decentration [mm]	Tilt [deg]	Angle of contact [deg]
Model A hydrophilic	2.049	1.91	0.012	0.22	127°76'
Model A hydrophobic	3.172	1.91	0.016	0.07	131°03'
Model B hydrophobic	0.518	1.72	0.28	1.07	86°31'
Model C hydrophobic	4.143	1.39	0.005	0.18	94°30'
Model D hydrophobic	0.990	1.20	0.012	0.16	91°86'

Table 4 Drop of the area under MTF with respect to the initial MTF value (initial denotes the case, where all the displacement parameters are set to zero). The area under the MTF has been calculated for two ranges of frequencies.

IOL model	Relative area under MTF for 0 to 30 cycles/deg	Relative area under MTF for 0 to 60 cycles/deg
	[%]	[%]
Model A hydrophilic	99.97	99.99
Model A hydrophobic	99.95	99.94
Model B hydrophobic	99.96	99.90
Model C hydrophobic	99.95	99.98
Model D hydrophobic	99.93	99.97

means all the displacement parameters set to 0). The area under the MTF was calculated for two ranges of frequencies, such as 0 to 30 and 0 to 60 cycles/deg.

Table 5 shows the values of Zernike coefficients estimated for the conditions of the initial (reference) and final configurations.

4 Discussion

In the present work, an *in silico* simulation evaluation of dynamic stability of different IOLs was performed using FEM software, according to the procedure described by the ISO 11979-3:2012.³⁵ To the best knowledge of the authors, it is the first time that the behavior of different IOL designs under dynamic compression conditions has been modeled using FEM. Two different materials and four different haptics designs and different overall diameters were analyzed. Additionally, the effect of lateral decentration and tilt of the IOL on the optical performance were studied in a model of a pseudophakic eye using a ray-tracing program. In the existing literature, the static biomechanical properties of different model IOLs were performed *in vitro* (laboratory investigation)^{4,9} and *in vivo* (rabbit)¹⁰ in the meaning of either static performance or diurnal changes.

Because of the complexity of the approach to the mechanical stability presented in the current study, including the experimental measurements of the mechanical properties of the materials, simulations of the behavior of the IOLs under dynamic compression tests, and the optical performance stimulation, we will briefly review below the most important findings of our investigations.

First of all, the mechanical properties of the IOL materials were experimentally evaluated in uniaxial compression test in saline bath. The results showed both the hydrophobic and hydrophilic materials manifested nonlinear characteristics, and the hydrophobic material was apparently stiffer than the hydrophilic one. Since the objective of the current study was to compare the response of different IOL models, for the purpose of this work we have modeled the stress–strain characteristics by means of the isotropic–incompressible hyperelastic model (see Fig. 4 and Table 2). The mechanical properties of the hydrophobic and hydrophilic materials measured in our study and used as input parameters for the numerical simulations were found similar to the ones measured experimentally by Bozukova et al.¹⁰

Another key parameter introduced in the FEM was the geometry of the IOLs, including the designs of their haptics (see Fig. 1). Before starting the simulations, the appropriate mesh for each type of element and the boundary conditions were analyzed (see Sec. 2 for more details).

The tests described in the ISO standards³⁵ have been analyzed numerically with the proposed FEM. The compression force applied by the IOL haptics to capsular bag (in this case to clamps) has been calculated for a well diameter of 10 mm (which can be associated with mean anatomic capsular bag size). This parameter is crucial for IOL rotational and refractive stability. Figures 5 and 6 show the behavior of the compression force and the axial displacement as a function of the clamp displacement for the same design of IOL and different material and the same material (hydrophobic) and different haptics design, respectively. Three different stages can be observed in these characteristics: (a) in the first stage the compression force increases and the axial displacement is hardly visible; (b) in the second stage, the compression force decreases rapidly and the axial displacement increases instantly. In this point, the IOL is released from the point of stability and the IOL wobbles rapidly. This stage takes some time and the plot of axial displacement has the form of the damped oscillations, and (c) the third stage is manifested as a slow and monotonic increase of the displacement with an increase in the force. This behavior can be observed for both materials (see Fig. 5), but it is subjected to the different haptic designs (see Fig. 6). We have found that the compression force simulated numerically for the hydrophilic IOL was slightly lower than for the IOL made of hydrophobic material for the same design of IOL. For model B (angular haptics), the first stage is not present and the axial displacement of the lens appears instantly when the force is applied. The second stage (oscillations associated to the release of the IOL) is less visible, and there is no drop in the compression force characteristic. For model C (plate haptics), the second stage (oscillations) is not present and the displacement characteristics are rather smooth with only one single point of discontinuity, associated with the presence of the maximum of the compression force. For model D (plate haptics with a hole), the characteristics are mixed: the first stage is clearly present; the second stage is manifested by oscillations of the force, but not in the axial displacement; and the third stage is present, but the force is kept constant. The largest compression force is manifested for the models A and C. The range of compression force variation was from 0.518 mN for the model B (angular haptics) to 4.143 mN for model C (plate). Bozukova et al.⁹ found a range of compression force variation between 0.34 and 3.65 mN, being higher for the IOLs with PMMA C-loops and plate hydrophilic acrylic haptics, followed by those with quadripod hydrophilic haptic. Lane et al.⁴ found a range of initial compression force variation between 0.25 and 3.89 mN with a rate of the compression force decay slowed over time (specially 24 h after compression) as a consequence of viscoelastic behavior. These results manifest that the compression force depends strongly on the model of the IOL and its material.

The maximum axial displacement was very similar in all the models of IOLs under consideration, in the range of 1.20 to 1.91 mm. For comparison, Lane et al.⁴ found a variation of the axial displacement between 0.15 and 1.98 mm, and they observed higher displacement values for the vaulted lenses. On the contrary, Bozukova et al.⁹ found displacement values

Table 5 Zernike coefficients (units in wavelengths) estimated using the pseudophakic eye model. The values in parentheses refer to the initial (reference) configuration, when no IOL displacement occurs.

IOL model	Z_2^0	Z_2^{-2}	Z_2^2	Z_3^{-1}	Z_3^1	Z_4^0
	Defocus	Astigmatism	Astigmatism	Coma	Coma	Spherical
Model A hydrophilic	0.029 (0.029)	-0.000016 (0.0)	0.0000052 (0.0)	-0.00064 (0.0)	0.00013 (0.0)	0.039 (0.039)
Model A hydrophobic	-0.0018 (-0.0020)	-0.000024 (0.0)	0.00010 (0.0)	0.00032 (0.0)	0.0020 (0.0)	0.045 (0.045)
Model B	-0.0029 (-0.0037)	0.00049 (0.0)	0.00055 (0.0)	-0.0012 (0.0)	-0.0052 (0.0)	0.047 (0.047)
Model C	-0.0024 (-0.0024)	0.000058 (0.0)	-0.000044 (0.0)	0.00012 (0.0)	0.00052 (0.0)	0.046 (0.045)
Model D	-0.0019 (-0.0020)	0.000060 (0.0)	0.000054 (0.0)	-0.00056 (0.0)	0.0014 (0.0)	0.045 (0.045)

smaller than in our study, within the range from 0 to 1.032 mm. The knowledge of the axial displacement is important to estimate the final position of the IOL inside the eye (effective length position) and to predict the IOL power, avoiding/minimizing

refractive “surprises.” The manufacturers incorporate this parameter in the A-constant for each model of IOL. Decentration and tilt are important factors that affect visual quality and higher order aberrations.³⁷ Table 3 shows the obtained

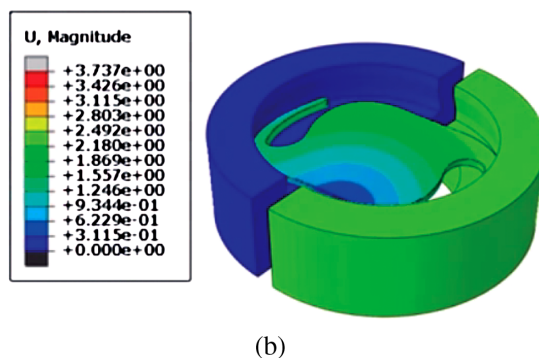
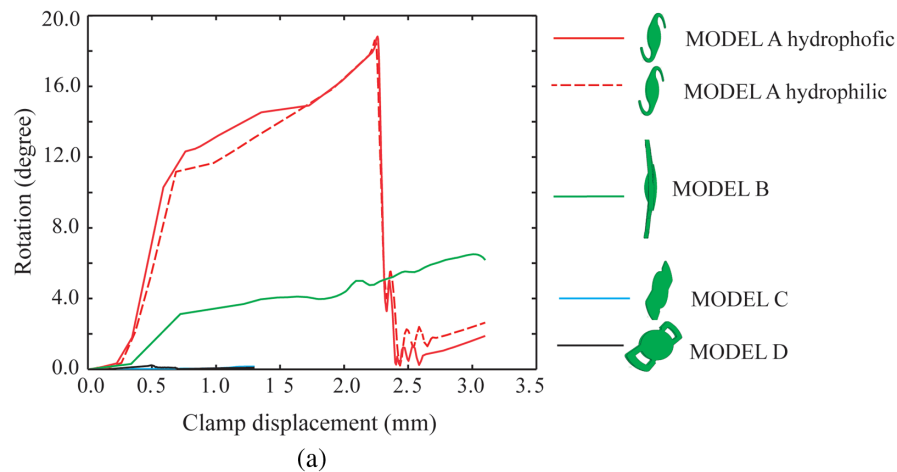


Fig. 8 (a) Evolution of rotation as a function of the clamp displacement for the different models of IOLs and (b) visualization of the behavior of the model A IOL under dynamic compression conditions. The map of colors is associated with the total dislocation of the nodes (Video 1, MP4, 767 KB [URL: <https://doi.org/10.1117/1.JBO.23.3.035003.1>]).

values in the final position, with a range of tilt variation between 0.22 deg and 1.07 deg and for decentration between 0.005 mm and 0.28 mm. It can be observed that the model B (angular haptics) has the less compression force and provides the highest decentration and tilt value. Bozukova et al.⁹ found higher tilt values within the range from 0 deg to 20.12 deg.

Another evaluated parameter was the angle of contact, and it is a measured approximation of the total haptic contact with the supporting ocular tissue. According to the earlier studies,¹⁰ a higher degree of haptic contact would be beneficial in preventing the IOL from rotation and misaligning. The variations for all evaluated models IOLs was between 86 deg and 131 deg (see Table 3). There is no difference between the same design of IOL and different material. The lowest angle of contact was for the model B (angular haptics).

The simulations of the optical performance show that only small changes in the modulation transfer function and aberrations in terms of Zernike coefficients occur when the final configuration (that means the magnitudes of displacement parameters, except the axial displacement, are taken from the last point of characteristics) is compared with the initial configuration (all the parameters of displacement are set to zero).

Although monofocal IOLs are still frequently employed in the treatment of cataract, the MIOLs and the T-IOLs are increasingly used modalities. Although the axial rotation—as a parameter—is not the subject of the ISO 11979-3 standard,³⁵ it is a major issue of T-IOLs and MIOLs with nonrotationally symmetric designs and rotational stability is of crucial importance for satisfying visual performance results. There are several factors that can cause the axial rotation, including incomplete viscoelastic clearance, early postoperative IOL fluctuations, misfit in capsulorhexis size, optic and haptic design, and the material of the IOL. In this study, we performed the additional analysis of the axial rotation for each IOL models. In a real pseudophakic eye, this kind of movement can be associated with the residual activity of the accommodation mechanism, which was proved³⁸ to be preserved after IOL implantation. Figure 8(a) shows these results as a function of the clamp displacement. It can be seen that plate-haptic IOLs are rotationally stable, whereas the C-loop designs undergo the axial rotation while increasing the compression force. The maximal magnitude of the rotation varies from 6 up to 18 deg and is significantly lower for model B (angular haptics) than for both models A. This is in agreement with the above comments regarding the compression force and angle of contact.

Figure 8(b) presents the visualization of the behavior of the model A IOL under dynamic compression conditions (please note that for better visualization of wobbling and rotation of the IOL, the time axis is not uniform).

In summary, we present a FEM as a versatile tool to evaluate numerically the biomechanical stability of different IOLs, according to the procedure described in the ISO standards.³⁵ We have demonstrated that FEM is a powerful tool to study the behavior of different IOLs and it allows an increase of the predictability of the cataract surgery and to help in the design phase to the manufacturers. In this study, only a capsular bag size, a one-piece IOL designs and a dioptric power (+22.00 D) have been considered, but the proposed method allows implementation of different capsular bags size, three-piece IOL (for example, IOLs with PMMA haptics), and dioptric powers and thickness of the IOL.

Disclosures

All the authors declare no conflicts of interest.

Acknowledgments

The authors gratefully acknowledge the support of Carlos III Health Institute (ISCIII) through the CIBER initiative as well as the financial support of the Ministerio de Economía y Competitividad, Projects: DPI2014-54981R and DPI2017-84047-R (MINICO-FEDER). L. Remón acknowledges Fundación Ibercaja-CAI (Grant No. CM02/7). The work was funded in cooperation with ICTS “NANBIOSIS”, specifically with the Tissue and Scaffold Characterization Unit (U13).

References

1. B. Cochener et al., “Comparison of outcomes with multifocal intraocular lenses: a meta-analysis,” *Clin. Ophthalmol.* **5**, 45–56 (2011).
2. E. Holland et al., “The AcrySof toric intraocular lens in subjects with cataract and corneal astigmatism: a randomized, subject-masked, parallel-group, 1-year study,” *Ophthalmology* **117**(11), 2104–2111 (2010).
3. S. K. Pandey et al., “Capsulorhexis ovaling and capsular bag stretch after rigid and foldable intraocular lens implantation: experimental study in pediatric human eyes,” *J. Cataract Refractive Surg.* **30**(10), 2183–2191 (2004).
4. S. S. Lane et al., “Comparison of the biomechanical behavior of foldable intraocular lens,” *J. Cataract Refractive Surg.* **30**(11), 2397–2402 (2004).
5. A. R. Vasavada et al., “Comparison of posterior capsule opacification with hydrophobic acrylic and hydrophilic acrylic intraocular lenses,” *J. Cataract Refractive Surg.* **37**(6), 1050–1059 (2011).
6. R. Duman et al., “Effect of four different intraocular lenses on posterior capsule opacification,” *Int. J. Ophthalmol.* **8**(1), 118–121 (2015).
7. A. Haripriya et al., “Long-term posterior capsule opacification reduction with square-edge polymethylmethacrylate intraocular lens. Randomized controlled study,” *Ophthalmology* **124**(3), 295–302 (2017).
8. A. Coombes and H. Seward, “Posterior capsular opacification prevention: IOL design and material [commentary],” *Br. J. Ophthalmol.* **83**(6), 640–641 (1999).
9. D. Bozukova, C. Pagnouille, and C. Jérôme, “Biomechanical and optical properties of 2 new hydrophobic platforms for intraocular lenses,” *J. Cataract Refractive Surg.* **39**(9), 1404–1414 (2013).
10. D. Bozukova et al., “Double-C loop platform in combination with hydrophobic and hydrophilic acrylic intraocular lens materials,” *J. Cataract Refractive Surg.* **41**(7), 1490–1502 (2015).
11. L. Remón et al., “Through-focus response of multifocal intraocular lenses evaluated with a spatial light modulator,” *Appl. Opt.* **51**(36), 8594–8598 (2012).
12. ISO 11979-2, “Ophthalmic implants - intraocular lenses. Part 2: optical properties and test methods,” International Organization for Standardization (2014).
13. C. K. Patel et al., “Postoperative intraocular lens rotation: a randomized comparison of plate and loop haptic implants,” *Ophthalmology* **106**(11), 2190–2196 (1999).
14. A. Prinz et al., “Rotational stability and posterior capsule opacification of a plate-haptic and an open-loop-haptic intraocular lens,” *J. Cataract Refractive Surg.* **37**(2), 251–257 (2011).
15. D. F. Chang, “Comparative rotational stability of single-piece open-loop acrylic and plate-haptic silicone toric intraocular lenses,” *J. Cataract Refractive Surg.* **34**(11), 1842–1847 (2008).
16. X. Zhong et al., “Comparisons of the in-the-bag stabilities of single-piece and three-piece intraocular lenses for age-related cataract patients: a randomized controlled trial,” *BMC Ophthalmol.* **16**, 100 (2016).
17. R. J. Linnola et al., “Adhesion of fibronectin, vitronectin, laminin, and collagen type IV to intraocular lens materials in pseudophakic human autopsy eye. Part I: histological sections,” *J. Cataract Refractive Surg.* **26**(12), 1792–1806 (2000).
18. R. J. Linnola, “Sandwich theory: bioactivity-based explanation for posterior capsule opacification,” *J. Cataract Refractive Surg.* **23**(10), 1539–1542 (1997).

19. T. Oshika, T. Nagata, and Y. Ishii, "Adhesion of lens capsule to intraocular lenses of polymethylmethacrylate, silicone, and acrylic foldable materials: an experimental study," *Br. J. Ophthalmol.* **82**(5), 549–553 (1998).
20. D. F. Chang, "Early rotation stability of the longer Staar toric intraocular lens: fifty consecutive cases," *J. Cataract Refractive Surg.* **29**(5), 935–940 (2003).
21. A. Venkataraman and Kalpana, "Visual outcome and rotational stability of open loop toric intraocular lens implantation in Indian eyes," *Indian J. Ophthalmol.* **61**(11), 626–629 (2013).
22. V. Gangwani et al., "Posterior capsule opacification and capsular bag performance of a microincision intraocular lens," *J. Cataract Refractive Surg.* **37**(11), 1988–1992 (2011).
23. D. A. Kumar et al., "Evaluation of intraocular lens tilt with anterior segment optical coherence tomography," *Am. J. Ophthalmol.* **151**(3), 406–412 (2011).
24. X. Wang et al., "IOL tilt and decentration estimation from 3 dimensional reconstruction of OCT image," *PLoS One* **8**(3), e59109 (2013).
25. M. Sun et al., "Intraocular lens alignment from an en face optical coherence tomography image Purkinje-like method," *Opt. Eng.* **53**(6), 061704 (2014).
26. J. Tabernero et al., "Predicting the optical performance of eyes implanted with IOLs to correct spherical aberration," *Invest. Ophthalmol. Visual Sci.* **47**(10), 4651–4658 (2006).
27. A. De Castro, P. Rosales, and S. Marcos, "Tilt and decentration of intraocular lenses in vivo from Purkinje and Scheimpflug imaging; validation study," *J. Cataract Refractive Surg.* **33**(3), 418–429 (2007).
28. S. Maedel et al., "Comparison of intraocular lens decentration and tilt measurements using Purkinje meter systems," *J. Cataract Refractive Surg.* **43**(5), 648–655 (2017).
29. J. T. Holladay et al., "A new intraocular lens design to reduce spherical aberration of pseudophakic eyes," *J. Refract. Surg.* **18**(6), 683–691 (2002).
30. S. S. Lane et al., "Multifocal intraocular lenses," *Ophthalmol. Clin. North Am.* **19**(1), 89–105 (2006).
31. G. Grabner, R. E. Ang, and S. Vilupuru, "The small-aperture IC-8 intraocular lens: a new concept for added depth of focus in cataract patients," *Am. J. Ophthalmol.* **160**(6), 1176–1184.e1 (2015).
32. R. Bellucci and M. C. Curatolo, "A new extended depth of focus intraocular lens based on spherical aberration," *J. Refractive Surg.* **33**(6), 389–394 (2017).
33. C. Canovas and P. Artal, "Customized eye models for determining optimized intraocular lenses power," *Biomed. Opt. Express* **2**(6), 1649–1662 (2011).
34. T. Eppig et al., "Effect of decentration and tilt on the image quality of aspheric intraocular lens designs in a model eye," *J. Cataract Refractive Surg.* **35**(6), 1091–1100 (2009).
35. ISO 11979-3, "Ophthalmic implants - intraocular lenses. Part 3: mechanical properties and test methods," International Organization for Standardization (2012).
36. D. A. Atchison, "Optical models for human myopic eyes," *Vision Res.* **46**(14), 2236–2250 (2006).
37. J. Landers and H. Liu, "Choice of intraocular lens may not affect refractive stability following cataract surgery," *Clin. Exp. Ophthalmol.* **33**(1), 34–40 (2005).
38. J. Tabernero et al., "The accommodative ciliary muscle function is preserved in older humans," *Sci. Rep.* **6**, 25551 (2016).

Laura Remón is an assistant professor at the University of Zaragoza. She received her BS and MS degrees in optics and optometry from the University of Valencia in 2004 and 2008, respectively, and her PhD in optics from the University Polytechnic of Valencia in 2012. She is the author of more than 18 journal papers. Her current research interests include optical design, and assessment of the optical quality.

Damian Siedlecki is an assistant professor at the Wrocław University of Science and Technology (WUST). He received his MS degree in biomedical engineering from WUST in 2001 and his PhD degree in physics from the Institute of Physics, WUST, in 2005. In 2017, he successfully completed his habilitation procedure. He is the author of more than 30 scientific papers and SPIE proceedings. His current research interests visual and physiological optics, including modeling, simulations, and experimental testing.

Iulen Cabeza-Gil is a master student at the University of Zaragoza. He received his BS degrees in engineering in 2017.

Begoña Calvo is a professor in the Department of Mechanical Engineering, Universidad de Zaragoza (UZ), Spain, since 2010. She is a member of the Aragón Institute of Engineering Research and the National Networking Center on Bioengineering, Biomaterials and Nanomedicine. Her current research is related to computational biomechanics, mainly in the field of mechanics of soft tissues, mechanical behavior of biomaterials, and prostheses for clinical procedures. She is the author of more than 80 journal papers.